Control of interlayer spacing in $(Pb_2Cu)Sr_2(Dy,Ce)_nCu_2O_{6+2n-z}/(Pb_2Cu)Sr_2Dy_{1-y}Ca_yCu_2O_{8+w}$ superconducting superlattices

Sumio Ikegawa, Kohei Nakayama, and Yuichi Motoi

Corporate Research & Development Center, Toshiba Corporation, 1, Komukai Toshiba-cho, Saiwai-ku, Kawasaki 212-8582, Japan

Masao Arai

National Institute for Materials Science, Tsukuba, Ibaraki 305-0044, Japan

We report on superconducting superlattices in which the distances between the superconducting layers are controlled at the shortest intervals so far achieved. This was accomplished by the artificial modification of an atomic layer stacking in the crystal structure of $(Pb_2Cu)Sr_2Dy_xCe_{n-x}Cu_2O_{2n+6}$ (Pb-$32n2$ phase: $n=3-8$), utilizing the tendency to self-organize a layered structure. *Ab initio* electronic structure calculations for the Pb-$32n2$ phase with $n=1-3$ suggest that the anisotropy of conduction increases with n. In $[(Pb-32n2)_1(Pb-3212)_3]_9$ ($n=3, 4, 6$) superconducting superlattices, the activation energy of flux motion decreases with increasing n. The above observations and the change in the shape of resistive transitions suggest that the interlayer coupling decreases with increasing the distances between the superconducting layers, as expected. We discuss coupling mechanisms.

I. INTRODUCTION

Atomic layer engineering for tailoring the properties of high-T_c cuprate superconductors and related oxides has been developed in the last decade.[1,2] This technology is based on the atomic layer-by-layer growth of thin films. From now on, atomic-layer engineering is expected to be developed with a view to realizing multifunctional oxide electronics devices including sensors, processors, and memories, which will be epitaxially integrated on a single crystal,[1,2] and its importance is bound to grow in the context of nanotechnology.

One of the properties of cuprate superconductors worth modifying is the interlayer Josephson coupling. The cuprate superconductors can be regarded as stacks of intrinsic Josephson junctions, because of their layered crystal structure.[3] The intrinsic junctions offer high performance, such as high I_cR_N product and superconductor-insulator-superconductor tunnel characteristics. However, the series array of the same junctions alone is of limited use for electronic applications: technologies for making a single junction at any place are needed. Thus the control of Josephson coupling in the arbitrary unit cell of layered cuprates is desirable in electronic applications. This should be accomplished by the artificial modification of an atomic layer stacking in the crystal structure, utilizing the tendency to self-organize a layered structure. Apart from the applications, an arbitrary control of interlayer Josephson coupling offers unique opportunities to study the mechanism of superconductivity and vortex dynamics.

In $(Pb_2Cu)Sr_2(Ln,Ce)_nCu_2O_{6+2n-z}$ ($n \geq 2$, Ln = trivalent rare-earth element) (Pb-$32n2$ phase), which is a layered cuprate having a multiple fluorite-type block layer, the spacing between a pair of CuO_2 planes can be arbitrarily chosen. So, the Pb-$32n2$ family offers the potential to control electronic anisotropy or the strength of the interlayer

Josephson coupling.[4] We successfully grew epitaxial films of Pb-$32n2$ with $n=3-8$ by the atomic layer-by-layer molecular beam epitaxy (MBE) technique.[4] The Pb-$32n2$ phases with $n>4$ are essentially impossible to obtain in pure phase form with bulk processes, since all these phases are energetically very close. In a previous paper,[5,6] we reported the in-plane transport properties of Pb-$32n2$ films with $n=3$ and 5. The Pb-$32n2$ phases with $n>2$ have not exhibited superconductivity to date. So, we have made a multilayer of the $(Pb_2Cu)Sr_2Dy_{1-y}Ca_yCu_2O_{8+w}$ (Pb-3212 phase) superconductor and the Pb-$32n2$ phase with $n>2$ to investigate how the anisotropy of superconductivity is affected by changing the interlayer spacing.

Taking advantage of the naturally layered structure, high-T_c multilayer structures have been extensively studied.[7,8] They offer the possibility of modifying in a systematic way some specific properties of high-T_c superconductors, such as vortex dynamics. Various superlattices have been reported, such as $YBa_2Cu_3O_7/PrBa_2Cu_3O_7$ (YBCO/PBCO), $Bi_2Sr_2CaCu_2O_8/Bi_2Sr_2Cu_2O_6$, and $YBa_2Cu_3O_7/SrRuO_3$. In these superlattices, the thickness of the spacer material was restricted to an integral multiple of the c-axis length, for example 1.2 nm for PBCO. The shortest unit length was a lattice parameter of a perovskite primitive cell (~ 0.39 nm). For the superlattices, the two materials should be compatible chemically, crystallographically, and electronically.[1] Since not every combination of oxides satisfies the above three conditions, careful selection is needed. Regarding various multilayer structures, variations in conductivity T_c and vortex dynamics have been discussed in terms of the coupling between the superconducting layers.[8] However, the mechanisms and effects of interlayer coupling, including the long-range proximity effect, are still subject to debate.[1,7,8] Therefore further studies on other systems are needed.

In this paper, we report interesting superlattices in which the distances between the superconducting layers are con-

trolled at the shortest intervals so far achieved. This work reveals that Pb-$32n2$ compound with $n>2$ and Pb-3212 superconductor are a suitable combination for the superconducting superlattices. The studies of crystal structure using x-ray diffraction, reflection high-energy electron diffraction, and transmission electron microscopy indicate chemical and crystallographic compatibility. The resistance measurements show superconductivity of the superlattices and, consequently, chemical and electronic compatibility. Finally, we report successful control of the interlayer coupling of superconductivity by changing the interlayer distance at the shortest intervals so far achieved. The coupling mechanisms are discussed. Preliminary results were published elsewhere.[9]

II. MATERIALS OVERVIEW

The Pb-$32n2$ phase with $n>2$ has multiple-stacked fluorite block layer, $[(Ln,Ce)O_2]_n$ (Ln is a trivalent rare-earth element), between a pair of CuO_2 planes in its crystal structure. This block layer probably acts as an insulator. The Pb-$32n2$ family is a unique system in that the distance d between the bases of a pair of pyramidal Cu-O planes across the fluorite block can be changed with a unit thickness of 0.27–0.28 nm through changing the layer number n of the rare-earth oxide. This interval corresponds to half of the lattice constant of CeO_2. Structural chemistry and in-plane transport properties of the Pb-$32n2$ phase films with $n=3, 5$ were reported in Ref. 5. Recently, the electronic structures of the Pb-3222 and Pb-3232 phases were calculated and were compared with those for the Pb-3212 phase.[10] The calculations were done within the local-density approximation, using the WIEN97 package,[11] which is based on the full-potential linear augmented plane-wave method.

Our chief concern is the change in transport properties and electronic anisotropy with increasing the distance between a pair of CuO_2 planes. The Fermi velocities parallel ($\nu_\parallel$) and perpendicular ($\nu_\perp$) to the CuO_2 plane were quantitatively evaluated from the calculated energy bands. The $\nu_\parallel$ values are 3.9×10^7 and 3.5×10^7 cm/s for Pb-3212 and Pb-3232, respectively. These values are comparable with those for other high-T_c superconductors.[12] The calculations showed that the antibonding bands of Cu $3d_{x^2-y^2}$ and O $2p$ orbitals have similar in-plane dispersion for the Pb-3212, Pb-3222, and Pb-3232 phases.[10] These results suggest that in-plane transport properties are insensitive to the distance between a pair of CuO_2 planes. Experimentally, the sheet conductance per CuO_2 plane was estimated from the resistivity data and was similar for the Pb-3232 phase and Pb-3252 phase.[5] This means that the strength of localization does not increase when the distance between a pair of CuO_2 planes d increases from 0.87 to 1.44 nm.[5]

The electronic anisotropy was evaluated from the ratio $\nu_\perp/\nu_\parallel$. The $\nu_\perp/\nu_\parallel$ values are 0.13 and 0.03 for Pb-3212 and Pb-3232, respectively. If the anisotropy of conductivity were naively estimated from $(\nu_\perp/\nu_\parallel)^2$, the anisotropy of Pb-3232 would be larger than that of Pb-3212 by one order of magnitude. Therefore the Pb-$32n2$ family is useful for the purpose of changing the c-axis transport while the in-plane transport is kept constant. Utilizing this family, we tried to

control the anisotropy of the superconductivity. The results are shown in the following.

III. EXPERIMENT

Thin films were grown by sequential deposition using the molecular beam epitaxy (MBE) apparatus. The MBE growth of the Pb-3212 superconductor[13,14] and the Pb-$32n2$: $n=3-8$ phase[4] was previously reported. So, we briefly describe the sample preparation. Pb, Sr, Dy, Ce, Ca, and Cu metals were evaporated from the effusion cells onto a $SrTiO_3$(001) surface. The surface structure and growth mechanisms have been investigated by *in situ* reflection high-energy electron diffraction (RHEED). We have synthesized superlattices of alternating one-unit-cell-thick layers of the Pb-$32n2$ phase $[(Pb_2Cu)Sr_2Dy_xCe_{n-x-\delta}Cu_2O_{2n+6-z}$: $n=3-7$, $x=1.4]$ with two- or three-unit-cell-thick layers of Pb-3212 superconductor $[(Pb_2Cu)Sr_2Dy_{1-y}Ca_yCu_2O_{8+w}$: $y=0.4]$, which are expressed as $[(Pb\text{-}32n2)_1(Pb\text{-}3212)_m]_k$: $m=2-3$, $k=9-13$. The crystal structure of one cycle for $n=3$, $m=3$ is shown in Fig. 1. Here and in the rest of this paper, we express the unit cell from the bottom Cu(1) site in the [SrO-PbO-Cu-PbO-SrO] block layer to the top Cu(1) site for convenience of explanation, as shown in Fig. 1. It should be noted that cation deficiency δ within the range between 0.3 and 1.2 exists in the fluorite block of Pb-$32n2$ phase films with $n=3-8$.[5] Growth conditions, such as the growth temperature and the oxygenation conditions during growth and during the cooling process after growth, were previously optimized for the Pb-$32n2$ phase.[5,15] In this study, the conditions were finely tuned for obtaining reproducible superconductivity in the superlattices. During growth, the substrate temperature was kept constant at 943 K and pure ozone gas was supplied to the substrate: the flux density of O_3 molecules was estimated to be 6×10^{18} sec^{-1} m^{-2} on the substrate.

The chemical composition of the films was evaluated from the metal flux densities just before the deposition, the durations of shutter opening, and the chemical analysis by inductively coupled plasma emission spectroscopy for other samples deposited under similar conditions. The evaluated compositions for $[(Pb\text{-}32n2)_1(Pb\text{-}3212)_3]_9$ superlattices are shown in Table I as the number of atoms per *ab*-plane unit cell area (0.148 nm^2) per shuttering cycle for each phase. In the films, Pb was about 30% deficient in terms of the stoichiometric composition.[13] The Sr-rich and Cu-deficient conditions were chosen to prevent the precipitation of Cu_2O.[13,14] The cation deficiency δ in the fluorite block of the samples in Table I was within the range between 0.4 and 0.8. Cu composition per unit cell was controlled at 96–100% of the stoichiometric value, as shown in Table I. The composition of Dy plus Ca per Pb-3212 unit cell was controlled at 100–105% of the stoichiometric value.

After the film growth, the phases present and lattice parameters were determined by x-ray diffraction (XRD), using Cu-$K\alpha$ radiation. The structure of the layers was studied using high-resolution transmission electron microscopy. Resistance measurements were carried out by a conventional dc four-probe method in the temperature range between 1.5 and
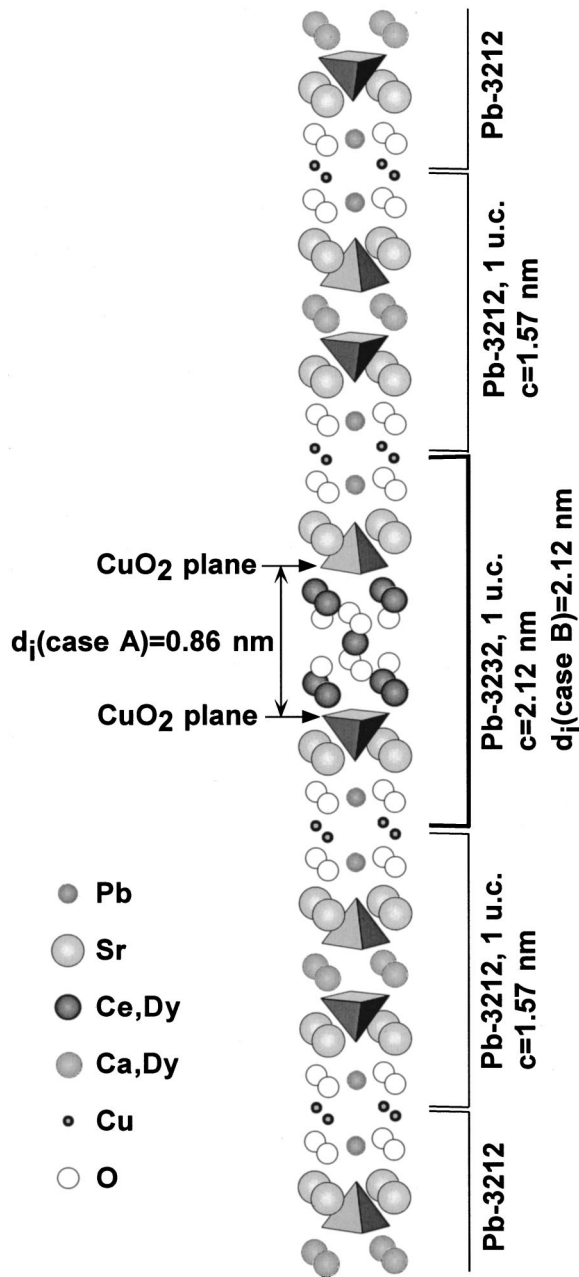
FIG. 1. Crystal structure for one cycle of $[(Pb\text{-}3232)_1(Pb\text{-}3212)_3]_9$ superlattices.
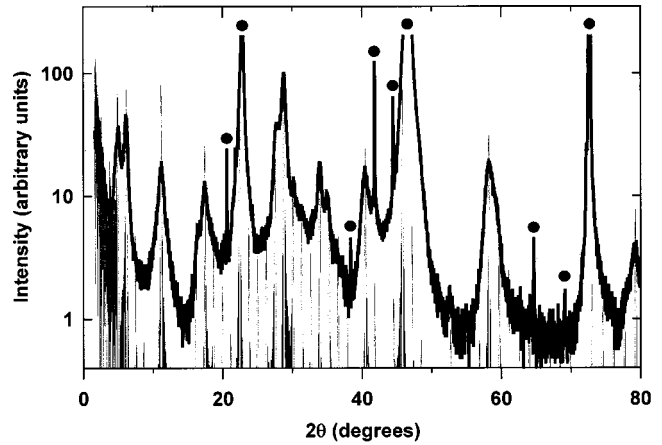
FIG. 2. XRD pattern for $[(Pb\text{-}3242)_1(Pb\text{-}3212)_3]_9$ superlattices. Thick black line indicates the experimental result. Thin gray line indicates the calculated diffraction pattern. Both patterns are normalized to 100 at the main peak of $2\theta = 28.8°$. Closed circles indicate the peaks due to the substrate.

field. The sample holder can be rotated relative to the magnetic field with accuracy better than 0.1°.

IV. RESULTS AND DISCUSSION

A. Crystal structure

First, we show the results of x-ray diffraction. The XRD pattern for $[(Pb\text{-}32n2)_1(Pb\text{-}3212)_3]_9$: $n = 4$ superlattices is shown in Fig. 2. The thick black line indicates the experimental result. The thin gray line indicates the calculated diffraction pattern assuming the ideal crystal structure.

From the experimental XRD patterns, the c-axis length for the superlattices c_{exp} which is a thickness of one cycle, was obtained by the least-square method. The results are shown in Fig. 3 and Table II. In Table II, $n = 1$, $m = 3$, and $L = 9$ represent the Pb-3212 single-phase film with 36-unit-cell thickness. Assuming the ideal crystal structures, which we will describe in the next paragraph, the c-axis lengths c_{ideal} were calculated as shown in Table II. In the calculation, n values were chosen according to the design, which were consistent with the compositions in Table I. The values of c_{exp} agree well with c_{ideal} within the experimental error.[16] The slope of the first-order linear regression of Fig. 3(a) is 0.275 nm per $\Delta n = 1$. The slope of the line through two data points of Fig. 3(b) is 0.275 nm per $\Delta n = 1$. These slopes are consistent with the expected value.[17] Thus the periodic structures were obtained just as intended. Next, we examine the interior of one cycle.

An XRD pattern for the following ideal crystal structure was calculated taking into account the Laue function, the

300 K. Resistivity was also measured under an applied field of 0.03–10 T using a superconducting solenoid. The current was parallel to the CuO$_2$ plane. The sample temperature was measured by using the calibrated Cernox sensor (Lake Shore Cryotronics Inc.), which was hardly affected by the magnetic

TABLE I. The evaluated compositions for $[(Pb\text{-}32n2)_1(Pb\text{-}3212)_3]_9$ superlattices.

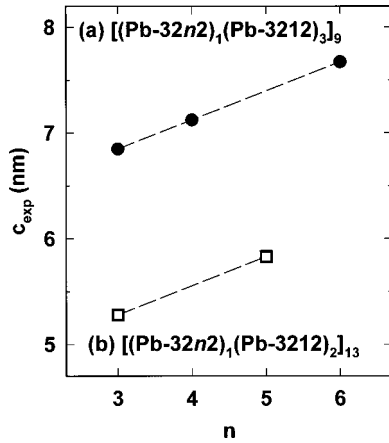| n	Pb-32n2 phase	Pb-3212 phase
3	$Pb_{1.4}Sr_{2.0}Dy_{1.44}Ce_{1.10}Cu_{2.99}O_y$	$Pb_{1.4}Sr_{2.0}Dy_{0.62}Ca_{0.43}Cu_{2.99}O_y$
4	$Pb_{1.4}Sr_{2.5}Dy_{1.41}Ce_{1.79}Cu_{2.90}O_y$	$Pb_{1.4}Sr_{2.5}Dy_{0.60}Ca_{0.45}Cu_{2.90}O_y$
6	$Pb_{1.4}Sr_{2.4}Dy_{1.41}Ce_{3.94}Cu_{2.97}O_y$	$Pb_{1.4}Sr_{2.4}Dy_{0.61}Ca_{0.44}Cu_{2.97}O_y$

FIG. 3. The experimentally obtained c-axis length for superlattices. (a) $[(\text{Pb-}32n2)_1(\text{Pb-}3212)_3]_9$: $n = 3-6$ superlattices. The line for (a) shows the first-order linear regression. (b) $[(\text{Pb-}32n2)_1(\text{Pb-}3212)_2]_{13}$: $n = 3, 5$ superlattices.

structure factor, the Lorentz factor, and the absorption factor for a finite-thickness film. In the calculation, we referred to Cava *et al.* for the crystal structure of the Pb-3212 phase.[18] The atom positions for the Pb-$32n2$ phase with $n = 3-6$ were estimated based on the Pb-3212 structure as follows.[4,5,10] The atom positions of the double fluorite block, $[(Ln,\text{Ce})\text{O}_2]_3$, were reported by Wada *et al.*[19] The positions for the multiple fluorite block were extrapolated by the insertion of the CeO_2 layers in the center of the double fluorite block. The multiple fluorite block were inserted between the CuO_2 planes in place of the (Ln,Ca) layer of the Pb-3212 structure. Finally, we took into account the difference in the ionic radius for different Ln^{3+}.[10] The peak positions and the relative intensities of measured XRD pattern (thick black line in Fig. 2) qualitatively agree with those of the calculated one (thin gray line in Fig. 2). The experimentally obtained XRD patterns for other superlattices of $[(\text{Pb-}32n2)_1(\text{Pb-}3212)_m]_k$ with $n = 3-7$, $m = 2-3$, $k = 9-13$ also qualitatively agreed with the calculated patterns assuming the ideal crystal structure. This suggests that desired crystal structure of superlattices was obtained at least

concerning their average structure. However, significant broadening of the measured diffraction peaks was observed as seen in Fig. 2. There may be several reasons for the broadening.

Before discussing the superlattices, we have to look back at the XRD patterns for the Pb-$32n2$ single-phase samples. The diffraction peaks of Pb-3252 and Pb-3232 single phases reported in Ref. 5 were broad in the experimental data compared with the simulated "ideal" XRD spectrum. In the film samples, several kinds of defect may exist such as Pb vacancies up to 30%, cation vacancies in the fluorite block with the amount of δ, and possible occupation of surplus Sr in the Pb sites. Intergrowth of the unit cell with different n value, which was frequently observed in the TEM photograph of bulk samples,[20] may also exist in the film sample. Random distributions of these defects are the reason for the broadening of the diffraction peaks for the Pb-3252 and Pb-3232 phases. This is also true for the present superlattices.

Additionally in superlattices, interfacial disorder has to be considered.[21] In the superlattices of the layered cuprate, there are two major kinds of interfacial disorder:[22] (i) steps of integer number of unit cells and (ii) interdiffusion of the different constituent elements in the two components: Ca and Ce for the Pb-3212 and Pb-$32n2$ ($n>2$) phases, respectively. These interfacial disorders bring about the broadening of the diffraction peaks. Disorder (i) with one-unit-cell height is inevitable with the present technology. Disorder (ii) may be present to a certain extent but is so weak that superconductivity in the Pb-3212 layer survives as will be shown later in Sec. IV B. In principle, many kinds of structural disorder in superlattices can be quantitatively determined by fitting the XRD profiles.[21–23] In the present case, however, it is too complicated to analyze in terms of the structural refinement since the broadening arises from both disorder within the Pb-$32n2$ and Pb-3212 phases and interfacial disorder of superlattices.

Next, we show RHEED observations during growth of the superlattices. Two-dimensional epitaxial growth was observed for the superlattices, as was the case for the Pb-3212 single phase[13] and Pb-$32n2$ single phase.[5] Figures 4(a) and (b) show typical oscillation of RHEED intensity during

TABLE II. The lattice parameter c and the thickness of insulating layer d_i and superconducting layer d_s for $[(\text{Pb-}32n2)_1(\text{Pb-}3212)_m]_L$ superlattices. c_{exp} and c_{ideal} are the experimentally obtained values and the calculated values assuming the ideal crystal structure, respectively. d_i and d_s are estimated for the ideal crystal structure in two cases. In case A, we assume that d_i is the distance between the CuO_2 planes across the fluorite block in the Pb-$32n2$ phase. In case B, the c-axis length for Pb-$32n2$ is regarded as d_i. $d_s = c_{\text{ideal}} - d_i$ in each case.

					Case A		Case B	
n	m	L	c_{exp} (nm)	c_{ideal} (nm)	d_i (nm)	d_s (nm)	d_i (nm)	d_s (nm)
1	3	9	1.575 ± 0.002	1.573				
3	3	9	6.85 ± 0.01	6.84	0.86	5.98	2.12	4.72
4	3	9	7.12 ± 0.02	7.11	1.13	5.98	2.39	4.72
6	3	9	7.67 ± 0.02	7.66	1.67	5.98	2.94	4.72
3	2	13	5.28 ± 0.02	5.27	0.86	4.41	2.12	3.15
5	2	13	5.83 ± 0.01	5.81	1.40	4.41	2.66	3.15

FIG. 4. RHEED observations during growth of $[(Pb\text{-}3242)_1(Pb\text{-}3212)_3]_9$ superlattices. (a) Intensity of the spot as a function of time; (b) intensity of the streak as a function of time. The bars below the curves indicate the interval while each shutter was open. (c) RHEED pattern after the deposition of the CuO_2 plane and just before the deposition of fluorite block; (d) RHEED pattern after the deposition of fluorite block; (e) RHEED pattern after the deposition of Pb oxide; (f) RHEED pattern after the deposition of the CuO_2 plane of Pb-3212 phase. The time instant for patterns (c)–(f) are shown in the upper panel.

growth of the $[(Pb\text{-}32n2)_1(Pb\text{-}3212)_3]_9$: $n=4$ superlattices. During the deposition of Pb-3212 layer, the RHEED intensity oscillates with a period of one unit cell while the streak pattern is retained. The intensity decreases during the deposition of Pb oxide, suggesting disordered surface layer of Pb oxide,[13] and increases during the deposition of Cu and other elements. During the deposition of the Pb-3242 unit cell, an additional feature appears. The spot pattern was superposed on the streak pattern during the deposition of fluorite block $[(Dy, Ce)O_2]_n$ as shown in Fig. 4(d), suggesting the formation of islands on the surface. This spot pattern is similar to the case of island growth of (100)-oriented CeO_2 film with {111} facet. The intensity of the spot (a) increases during the deposition of fluorite block. In the next stage, during deposition of Pb oxide, the intensity of the spot de-

FIG. 5. Cross-sectional TEM image of $[(Pb\text{-}3242)_1(Pb\text{-}3212)_3]_9$ superlattices. Horizontal arrows indicate [PbO-Cu-PbO] block layers. Three cycles of the same structure, which correspond to three unit cells of Pb-3212 phase, are clearly visible.

creases. After the deposition of Pb oxide, the RHEED pattern becomes faint streaks as shown in Fig. 4(e). After deposition of the next CuO_2 plane, the streak pattern without superposition of the spot pattern is restored [Fig. 4(f)] to its original shape [Fig. 4(c)]. This indicates the tendency to self-organize a layered structure which distinguishes the Pb-$32n2$ phase from the simple CeO_2 insulator. The RHEED oscillations during growth of Pb-3242 and Pb-3212 single phases were reported in Fig. 2 of Ref. 5 and Fig. 4 of Ref. 13, respectively. The RHEED oscillation for the superlattices in Figs. 4(a) and (b) appears to be a combination of the oscillation for the Pb-3242 single phase and that for the Pb-3212 single phase. This means that each unit cell in the superlattices grew just like in the single-phase sample.

A cross-sectional transmission electron microscopy (TEM) was used to study the structure of the layers of the samples. The TEM image of the superlattices with $n=7$, $m=2$, $k=15$ in the previous paper[5] showed regularly aligned dark bands, which corresponded to the fluorite block layers, and agreed with the desired structure. In this paper we observed the superlattices with $n=4$, $m=3$, $k=9$ by TEM. The TEM image of this sample was also characterized by the regularly aligned dark bands, which corresponded to the fluorite block layers. The periodic structure agreed well with the plan. In the sample preparation for cross-sectional TEM, the fluorite block is harder to be thinned by the ion-milling than the other part of the superlattices. Then the periodic contrast was visible and the dark bands appeared in the proximity of the fluorite blocks. In this paper, we made close observation between the dark bands. Figure 5 shows a high-resolution phase contrast micrograph between the two dark bands. Heavy atoms, such as Pb, appear to be dark in this figure. In Fig. 5, we can see four rows of black dumbbells as indicated by horizontal arrows, which correspond to the [PbO-Cu-PbO] block layer, between the upper and lower dark bands. Thus three cycles of the same structure, which correspond to three unit cells of the Pb-3212 phase, are clearly visible between the fluorite blocks, as designed.

The RHEED oscillations and TEM image show that there is no significant mixing between the Pb-32n2 phase with n >2 and the Pb-3212 phase. These results rule out the possibility of the superlattices consisting of different layers from the plan but having the same c-axis length.

The XRD, RHEED, and TEM experiments show that the superlattices were obtained as planned. This was accomplished after a precise control of the compositions per cycle as shown in Table I. The results indicate chemical and crystallographic compatibility between the Pb-32n2 (n>2) and Pb-3212 phases for making superlattices. The increase of the c-axis length by a unit length of 0.275 nm with increasing n indicates that the distance between the CuO$_2$ planes in the Pb-32n2 phase (n>2) increased by the same unit length. Namely, the distances between the superconducting layers are controlled at the shortest intervals so far achieved.

Superconducting superlattices consist of superconducting and nonsuperconducting layers. In the present superlattices, the range of superconducting order along the stacking direction is not clear at present. So we divide the c_{ideal} into two parts for a guide to picture the thickness of the superconducting layer d_s and nonsuperconducting layer d_i. A simple idea is that three times c-axis length for Pb-3212 is regarded as d_s. In this case, d_i, is the c-axis length for Pb-32n2. The estimated values of d_i and d_s assuming the ideal crystal structure are shown in Table II as case B. Case A in Table II is the case that the superconducting order parameter develops within the broadest range in the superlattices. Namely, d_i is the thickness of the fluorite block layer in the ideal structure, which is defined by the distance between the CuO$_2$ planes across the fluorite block, and d_s is the thickness of the rest in the one cycle of superlattices (see Fig. 1).

B. Resistive transition

The temperature dependence of resistivity for $[(\text{Pb-}32n2)_1(\text{Pb-}3212)_3]_9$ with $n=1, 3, 4, 6$ was measured under a zero field and an applied field parallel and perpendicular to the CuO$_2$ plane. The results are shown in Figs. 6 and 7. Here, $n=1$ represents the Pb-3212 single-phase film with 36 unit-cell thickness. As shown in Figs. 6 and 7, we successfully obtained superconductivity in the superlattices. In zero fields, the zero resistance state appeared at temperatures below 26.4, 2.01, and 2.04 K for $n=1, 3$, and 4, respectively. For $n=6$, the zero resistance state did not appear, which may be due to the limited temperature range of measurements ($T \geqslant 1.57$ K) and large superconducting fluctuations. We observed that the resistivity for the sample with $n=6$ decreased down to 5% of the normal-state value at 1.57 K and considered the sample as superconductor. Resistivity for each sample increases with increasing magnetic field, as in the case of an ordinary superconductor.

We now discuss the changes in the resistive transition depending on n from the following two points of view. Region I: the amplitude of superconducting order parameter is small and fluctuations in the amplitude are crucial to the energy dissipation. Roughly speaking, the temperature range where $\rho > A\rho_n$: $A = 0.2-0.7$, where ρ_n is normal-state resistivity, corresponds to region I.[24] Region II: the amplitude of
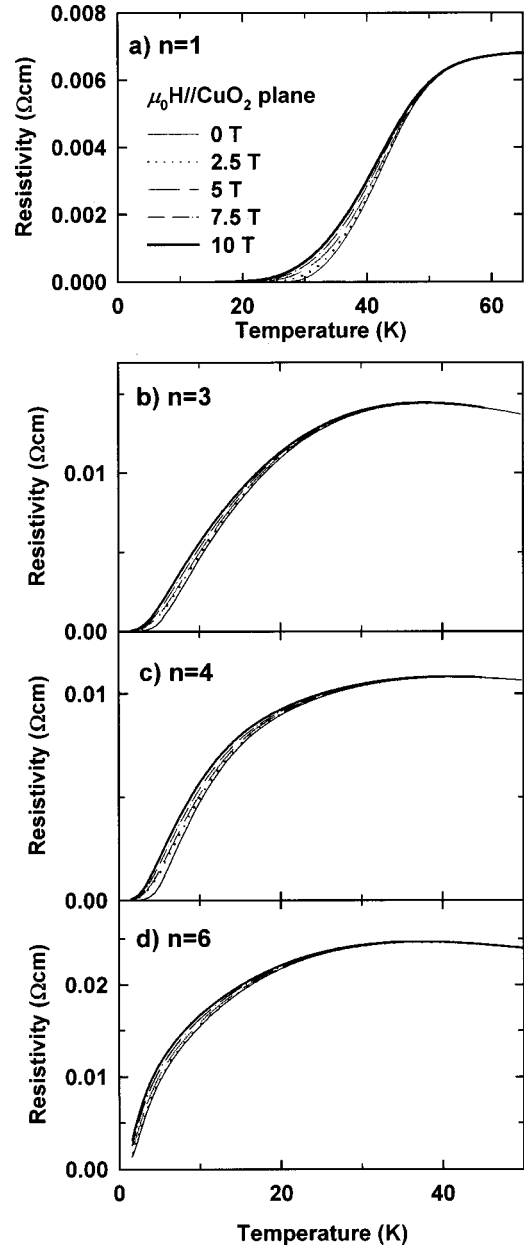

FIG. 6. Resistive transition under an applied field parallel to the CuO$_2$ plane for $[(\text{Pb-}32n2)_1(\text{Pb-}3212)_3]_9$ with $n=1, 3, 4, 6$ superlattices.

superconducting order parameter is well developed and the thermally activated flux flow (TAFF) dominates the energy dissipation under the magnetic field. Region II is approximately the temperature range where $\rho < B\rho_n$: $B \sim 0.01$.[25] Our purpose is to elucidate how the interlayer spacing affects the interlayer coupling of superconductivity, which consists of the Josephson coupling and magnetic coupling.

In a zero field, resistivity for $n=3, 4$, and 6 increases gradually with decreasing temperature from room temperature and exhibits maximum at around 40 K and then decreases with decreasing temperature, which indicates that the superconductivity starts to develop. Figure 8 shows the temperature T_{max} at which resistivity exhibits the maximum for the samples with $n=3-6$. T_{max} seems to be independent of
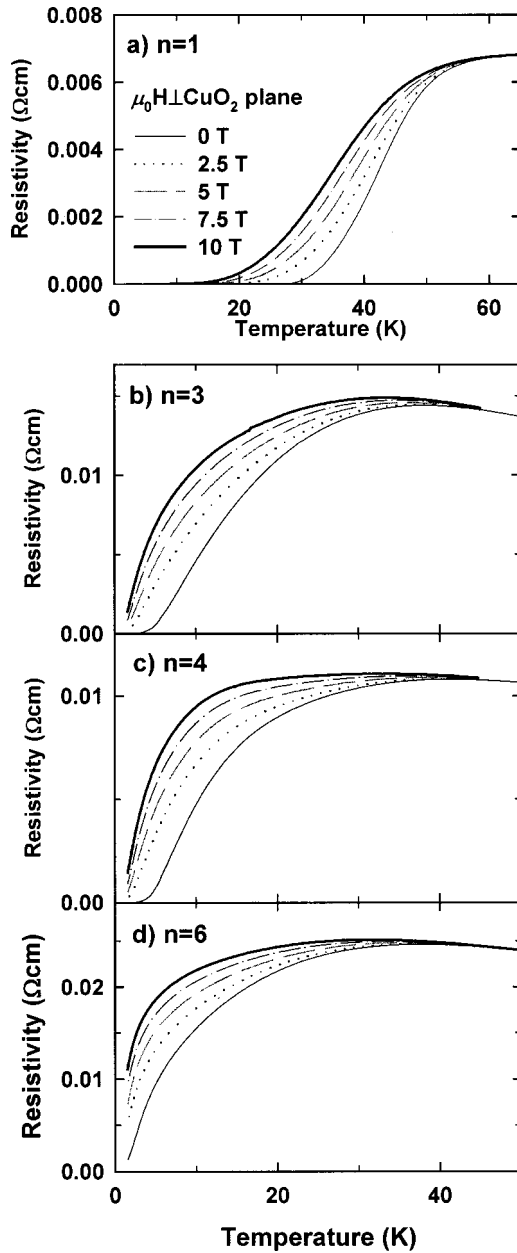
FIG. 7. Resistive transition under an applied field perpendicular to the CuO_2 plane for $[(Pb\text{-}32n2)_1(Pb\text{-}3212)_3]_9$ with $n=1, 3, 4, 6$ superlattices.

FIG. 8. The n dependence of characteristic temperatures for $[(Pb\text{-}32n2)_1(Pb\text{-}3212)_3]_9$ with $n=3, 4, 6$ superlattices. T_{max} is the temperature at which resistivity shows maximum. $T_c(0)$ and $T_c(10)$ are the critical temperatures, defined by the temperature at which resistivity drops 70% of the maximum value ρ_N under zero fields and an applied field of 10 T perpendicular to the CuO_2 plane, respectively. Lines are a guide for the eyes.

Fig. 7, it is conspicuous in the perpendicular magnetic field that the temperature width between T_{max} and T_c is expanded as n increases. In Fig. 8, the critical temperatures $T_c(10)$ under an applied field of 10 T perpendicular to the CuO_2 plane are also shown. It should be noted that the change of T_c definition, for example, to the temperature at which resistivity drops 50–90% of ρ_N, did not qualitatively alter the results: T_c decreases with increasing n.

The increase of the temperature width between T_{max} and T_c suggests that the fluctuations in the order parameter grow stronger with increasing n. This suggests that the interlayer Josephson coupling is considered to become weak with increasing n.

C. Activation energy

The activation energy U for flux motion was estimated using the Arrhenius plots of the resistivity data under the magnetic field, assuming that the thermally activated flux flow (TAFF) dominates the energy dissipation. U was estimated from each curve of resistive transitions under various magnetic fields for $[(Pb\text{-}32n2)_1(Pb\text{-}3212)_3]_9$ with $n=1, 3, 4,$ and 6. The data in the region where the viscous flow of the flux lines is dominant must be eliminated to estimate U. Basically, U was estimated from the data of $\rho < 0.01\rho_N$ in each curve. For the resistivity curve not to decrease down to $0.01\rho_N$ due to the limited temperature range of measurements, U was estimated from the data at $T < 2$ K and $\rho < 0.1\rho_N$. For the resistivity curve not to decrease down to $0.1\rho_N$ at 2 K, we could not estimate U. Thus obtained U values are larger than 2 K, which is consistent with our restriction on temperature range of the data used. Figure 9 shows one example of Arrhenius plots and the procedure for obtaining the activation energy $U(t)$. It should be noted that positive curvature was observed in the temperature range below the onset of superconductivity and above TAFF region in
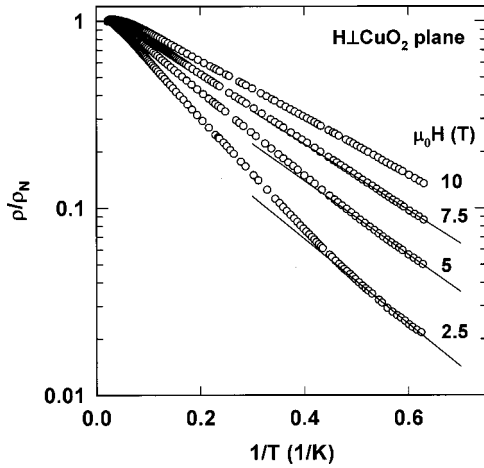
n, which implies that superconducting order starts at nearly the same temperature for the samples with $n=3\text{--}6$. Of course, T_{max} does not strictly represent the starting point of superconducting order and is a guide. Another guide for the starting point of superconducting order is the temperature, T_{semi}, at which resistivity separates from semiconducting thermal activation behavior on the high-temperature side. T_{semi} was 58–61 K and, like T_{max}, appeared to be independent of n for $n=3\text{--}6$. Figure 8 also shows the critical temperature in zero fields, $T_c(0)$, which was defined by the temperature at which resistivity drops 70% of the maximum value, ρ_N. The temperature width between T_{max} and $T_c(0)$ is expanded as n increases. This means that the temperature width of region I is expanded as n increases. As shown in

FIG. 9. Arrhenius plots of resistivity under various magnetic fields perpendicular to the CuO_2 plane for $[(Pb\text{-}3242)_1(Pb\text{-}3212)_3]_9$ superlattices. Lines show the first-order linear regression for evaluation of the activation energy.

the Arrhenius plots, unlike the case of YBCO/PBCO super-lattices. This behavior was also reported for $Bi_2Sr_2CaCu_2O_x$ (Ref. 26) and $HgBa_2Ca_2Cu_3O_{8+\delta}$.[27] Lines in Fig. 9 show the first-order linear regression to the data points that satisfy the above-mentioned conditions. $U(t)$ was obtained from the slope of the lines. The activation energy at $T=0$, U_0, was calculated by using a relation[28]

$$U(t) = U_0 \frac{(1-t^2)^q}{(1+t^2)q^{q-2}}, \tag{1}$$

where $t = T/T_c$. We employed one as the value of q.[29] The activation energy at $T=0$ in an applied field parallel and perpendicular to the CuO_2 plane is shown in Figs. 10 and 11, respectively.
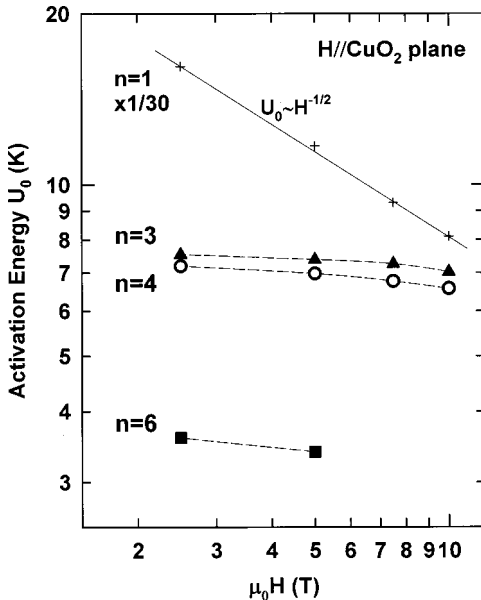
FIG. 10. Activation energy at $T=0$ under an applied field parallel to the CuO_2 plane for $[(Pb\text{-}32n2)_1(Pb\text{-}3212)_3]_9$ with $n=1, 3, 4, 6$ superlattices.
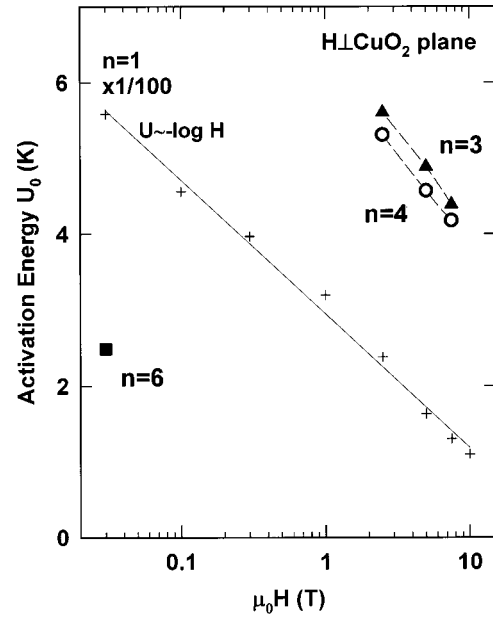
FIG. 11. Activation energy at $T=0$ under an applied field perpendicular to the CuO_2 plane for $[(Pb\text{-}32n2)_1(Pb\text{-}3212)_3]_9$ with $n=1, 3, 4, 6$ superlattices.

In the case of $H\|CuO_2$ plane (Fig. 10), U_0 for the Pb-3212 single-phase film ($n=1$) shows $U_0 \sim H^{-1/2}$, which is usually reported for YBCO films.[30] As shown in Fig. 10, U_0 for the superlattices with $n=3-6$ has weaker field dependence than that of the Pb-3212 single-phase film. This reflects the small thickness of superconducting layer in the superlattices,[8] in which the lower critical field H_{cl} is very large and the energy dissipation due to the flux motion hardly exists. H_{cl} is expressed as

$$H_{cl} = \frac{2\lambda_{ab}\phi_0}{\pi\lambda_c d_s^2} \ln\left(\frac{d_s}{\sqrt{\xi_{ab}\xi_c}}\right), \tag{2}$$

where λ_{ab}, λ_c, ξ_{ab}, and ξ_c are penetration depth and coherence length within the ab plane and for the c axis of the thin superconducting layer.[8] We used the reported values for the Pb-3212 single crystal: $\lambda_{ab}=257.5$ nm, $\lambda_c=642.5$ nm, $\xi_{ab}=1.85$ nm, and $\xi_c=0.3$ nm.[31] If we assume that all the portions except the fluorite block layers in the superlattices are superconducting, d_s is 5.98 nm (case A in Table II) and H_{cl} becomes 31 T. If we assume $d_s=4.72$ nm, which is a thickness of the three-unit-cell Pb-3212 phase (case B in Table II), H_{cl} becomes 44 T. If d_s is smaller than 4.72 nm, H_{cl} is larger than 44 T. Thus H_{cl} is larger than the maximum applied field (10 T). It should be noted for the case of $H\|CuO_2$ plane that the field-induced broadening of transition (Fig. 6) and hence a weak but finite field dependence of U_0 (Fig. 10) were observed at the field below H_{cl}. These results indicate the existence of interlayer Josephson coupling between the thin superconducting layers.

Here, we should pay attention to alignment of the magnetic field. Before the measurements for the $H\|CuO_2$ plane, we measured the dependence of resistivity on the angle be-

tween the sample surface and applied field H_{appl}, and the angle was set to minimize resistivity. Possible misalignment was 0.1°. Then, we estimated the effect of the c-axis component of magnetic field, $H_{\perp} = H_{appl} \sin(0.1°)$. The effect of $H_{\perp}$ on the resistivity was estimated to be smaller by more than one order of magnitude than that of $H_{\parallel} = H_{appl} \cos(0.1°)$. Therefore the field-induced broadening of transition (Fig. 6) and the field dependence of U_0 (Fig. 10) were not attributed to the c-axis component of magnetic field.

In the case of the $H \perp CuO_2$ plane (Fig. 11), U_0 for the Pb-3212 single-phase film ($n=1$) shows $U_0 \sim -\ln H$, which is usually reported for YBCO films and YBCO/PBCO superlattices.[8,32] For the superlattices with $n=3$ and 4, similar field dependence was observed although the field range was limited.

The values of U_0 for both the parallel (Fig. 10) and perpendicular (Fig. 11) fields decrease with increasing n. This suggests that the interlayer coupling in the superconducting superlattices, which consists of the Josephson coupling and magnetic coupling, is weakened with increasing n, as explained in the following. It should be noted that the differences in U_0 between the case of $n=3$ and 4 shown in Figs. 10 and 11 are meaningful, judging from the resistivity data.

In the TAFF model, each individual flux line is pinned in a potential well and is depinned by thermal activation. The latter process corresponds to the jump of a segment of length L_c of a flux line. The activation energy U_0 is proportional to the correlation length L_c, which is determined by a minimization of the cost in energy for a vortex segment to jump.[8] In the case of $H \perp CuO_2$ plane, the pancake vortices move along the CuO_2 plane. As d_i increases, interaction between the pancake vortices on the adjacent superconducting layers becomes weak, resulting in a decrease of L_c and U_0. In the case of $H \parallel CuO_2$ plane, magnetic fluxes enter the insulating layers. The activation process corresponds to the flux jump across the CuO_2 plane, which is dominated by the creation of a pancake vortex-antivortex pair at the CuO_2 plane. The smaller the distance d_i, the stronger the interlayer coupling is, resulting in raising of the energy barrier for the creation of the vortex-antivortex pair.

There is another possible explanation for the decrease of U_0 with increasing n, that is the decrease of d_s with increasing n. It causes the decrease in the correlation length L_c along the c axis, and hence the decrease in U_0 under a perpendicular field. In the case of the $H \parallel CuO_2$ plane, the decrease of d_s causes lowering of the energy barrier for the creation of the vortex-antivortex pair and, consequently, lowering of U_0. The superconducting fluctuations described in Sec. IV B may be enhanced with decreasing d_s. Then the experimentally obtained changes in the resistive transition depending on n can be explained by the changes in d_s. However, the design of the superlattices was intended to preserve d_s for different n values. The strength of localization in the CuO_2 plane did not increase with increasing n, as mentioned in Sec. II. Thus there is no evidence of decrease in d_s with increasing n.

D. Interlayer coupling mechanism

The experimental results show that the interlayer coupling of superconductivity is weakened as n increases. So, the kind of interlayer coupling that occurs has to be elucidated. It is helpful to compare the present system with the YBCO/PBCO superlattices, which have been thoroughly studied.[8,25,30,32] First, we discuss the existence of the magnetic interlayer coupling under a perpendicular field, which has been studied as the origin of the dc transformer during the last quarter of the 20th century.[33] In the case of YBCO/PBCO, the magnetic coupling was not observed since the energy of magnetic coupling is the order of T_c and much lower than the observed activation energy.[8] In the present case, U_0 is the order of T_c and we can expect to observe the magnetic coupling. The smaller U_0 may be caused by the stronger anisotropy in the Pb-3212 superconductor with rather lower doping than that of YBCO. In more detail, we have to consider the field dependence for the energy of magnetic coupling. Following Ekin and Clem,[33] the maximum coupling force can be written as

$$F_m = \frac{3\phi_0^2}{32\pi^3\lambda^4} \frac{[1 - \exp(-g_{10}d_s)]^2 \exp(-g_{10}d_i)}{g_{10}^2}, \quad (3)$$

$$g_{10} = (8\pi^2 B/\sqrt{3}\phi_0)^{1/2}, \quad (4)$$

where λ, d_s, and d_i are the penetration depth and the thicknesses of the superconducting and insulation layers, respectively. The maximum coupling force occurs when the displacement of vortex line is equal to one-fourth of the intervortex spacing d_v. So, we consider the maximum coupling energy E_m to be $F_m d_v/4$, which decreases with increasing H. E_m for the present superlattices is estimated using the value $\lambda_{ab} = 257.5$ nm,[31] as follows. If we use the values of case A in Table II for the values of d_i and d_s, E_m is 2.15–2.09 K under the field of 0.1 T for $n=3-6$. If we use the values of case B in Table II for the values of d_i and d_s, E_m is 2.07–2.03 K under the field of 0.05 T for $n=3-6$. Thus in the perpendicular field of less than 0.1 T, E_m is the order of the observed U_0 for $n=6$ and there is a possibility of observing the magnetic coupling in the present system (see Fig. 11). However, in the perpendicular field larger than 2 T, E_m is smaller than 0.2 K. Therefore the observed n dependence of U_0 for the perpendicular field larger than 2 T is not due to the magnetic coupling.

Second, we discuss whether the Josephson-like coupling exists or not. In the case of YBCO/PBCO, the activation energy for flux motion decreased with increasing PBCO thickness from 2.4 to 4.8 nm and the Josephson coupling is considered to exist across the 2.4-nm-thick PBCO.[25,32] From this, it is suspected that the Josephson coupling exists across the one-unit-cell thickness of Pb-32n2: $n=3-6$, which is 2.13–2.96 nm, and is weakened with increasing n. The weak but finite field dependence of U_0 under the parallel field (Fig. 10) and the increase of the temperature width between T_{max} and T_c with increasing n (Fig. 8) support the existence of Josephson coupling.

If the proximity effect (PE) acts on the CuO_2 planes in the Pb-32n2 phase with $n=3-6$, d_i becomes 0.86–1.67 nm (case A in Table II) and the Josephson coupling probably

exists between the CuO_2 planes judging from the distance. Previously, we investigated the possibility of the PE by comparing the transport properties of Pb-$32n2$ single phase with the theory for a two-dimensional dirty metal,[34] and we could not rule out the occurrence of PE.[5] On the other hand, the SO(5) theory of high-temperature superconductivity suggests that the range of PE in an underdoped nonsuperconducting layered cuprate is wider than the expected value from the conventional theory.[35] The Pb-$32n2$ phase with $n = 3-6$ is the underdoped nonsuperconducting layered cuprate. So, we can expect the occurrence of the PE on the CuO_2 plane in the Pb-$32n2$ phase and consequently the Josephson coupling across the fluorite block. In order to know the range of superconducting order along the stacking direction, further studies are needed: for example, the transport entropy per unit of vortex length can be obtained by measuring the Nernst effect[36] and its n dependence will provide us with valuable information. Furthermore, studies of c-axis transport for the multilayer are needed after making a mesastructure.

V. SUMMARY

We tried to control an atomic layer structure and, consequently, the interlayer coupling of superconducting superlattices. For this purpose, we have used the Pb-$32n2$ family, for which *ab initio* electronic structure calculations suggest that the anisotropy of conduction increases with n. Judging from the XRD, RHEED, and TEM studies, we have successfully grown the superconducting superlattices in which the distances between the superconducting layers are controlled at the shortest intervals so far achieved. The experimental results concerning the shape of resistive transition and the activation energy of flux motion indicate that the interlayer coupling across the fluorite block layer is controlled by changing the number of atomic layer n. Thus the Pb-$32n2$ phase with $n > 2$ and Pb-3212 superconductor is a suitable combination for the high-T_c multilayer structures.

ACKNOWLEDGMENTS

[1] I. Bozovic, IEEE Trans. Appl. Supercond. **11**, 2686 (2001).
[2] D. Pavuna, Curr. Appl. Phys. **1**, 9 (2001).
[3] R. Kleiner, F. Steinmeyer, G. Kunkel, and P. Müller, Phys. Rev. Lett. **68**, 2394 (1992).
[4] S. Ikegawa and Y. Motoi, Appl. Phys. Lett. **68**, 2430 (1996).
[5] S. Ikegawa and Y. Motoi, Phys. Rev. B **61**, 6334 (2000).
[6] S. Ikegawa and Y. Motoi, Physica C **341−348**, 1887 (2000).
[7] I. Bozovic and J. N. Eckstein, in *Physical Properties of High Temperature Superconductors V*, edited by D. M. Ginsberg (World Scientific, Singapore, 1996), p. 99.
[8] J. M. Triscone and Ø. Fischer, Rep. Prog. Phys. **60**, 1673 (1997).
[9] S. Ikegawa, Y. Motoi, and M. Arai, Trans. Mater. Res. Soc. Jpn. **26**, 1037 (2001).
[10] M. Arai and S. Ikegawa, Trans. Mater. Res. Soc. Jpn. **26**, 1001 (2001).
[11] P. Blaha, K. Schwarz, and J. Luitz, WIEN97, A Full Potential Linearized Augmented Plane Wave Package for Calculating Crystal Properties (Karlheinz Schwartz, Techn. Universität Wien, Austria, 1999). ISBN 3-9501031-0-4.
[12] P. B. Allen, W. E. Pickett, and H. Krakauer, Phys. Rev. B **37**, 7482 (1987).
[13] S. Ikegawa, Y. Motoi, and T. Miura, Physica C **229**, 280 (1994).
[14] Y. Motoi and S. Ikegawa, Appl. Phys. Lett. **73**, 987 (1998).
[15] S. Ikegawa and Y. Motoi, Physica C **282−287**, 673 (1997).
[16] There is possible deviation that c_{exp} is larger than c_{ideal} systematically. It can be explained by the enlargement of the distance between Pb and Cu(1) for 0–0.6%, since the excess oxygen usually extends the distance up to 10%. For the effects of excess oxygen on crystal structure, see M. Marezio, A. Santoro, J. J. Capponi, R. J. Cava, O. Chmaissem, and Q. Huang, Physica C **199**, 365 (1992).
[17] It should be noted that the slope of 0.275 nm is slightly larger than half of the lattice constant of CeO_2 ($= 0.271$ nm). The experimentally obtained c-axis length for the Pb-$32n2$ single phase with $n = 3-6$ is expressed as $c_{exp} = 0.273n + 1.319$ (nm). This slope is also slightly larger than half of the lattice constant of CeO_2. These discrepancies may arise from the substitution of large Dy^{3+} for Ce^{4+}.
[18] R. J. Cava, M. Marezio, J. J. Krajewski, W. F. Peck, Jr., A. Santoro, and F. Beech, Physica C **157**, 272 (1989).
[19] T. Wada, A. Ichinose, F. Izumi, A. Nara, H. Yamauchi, H. Asano, and S. Tanaka, Physica C **179**, 455 (1991).
[20] A. Tokiwa, T. Oku, M. Nagoshi, and Y. Shono, Physica C **181**, 311 (1991).
[21] E. E. Fullerton, I. K. Schuller, H. Vanderstraeten, and Y. Bruynseraede, Phys. Rev. B **45**, 9292 (1992).
[22] O. Nakamura, E. Fullerton, J. Guimpel, and I. K. Shuller, Physica C **185−189**, 2069 (1991).
[23] A. Vailionis, A. Brazdeikis, and A. S. Flodström, Phys. Rev. B **51**, 3097 (1995).
[24] Actually, resistive transition of cuprate superconductors for $\rho > A\rho_n$: $A = 0.2-0.7$ is well explained by the theoretical calculation of superconducting fluctuations. The value of A depends on magnetic field, anisotropy, and material parameters; see R. Ikeda, T. Ohmi, and T. Tsuneto, J. Phys. Soc. Jpn. **60**, 1051 (1991); **58**, 1377 (1989).
[25] J.-M. Triscone, L. Antognazza, O. Brunner, L. Mieville, M. G. Karkut, P. van der Linden, J. A. A. J. Perenboom, and Ø. Fischer, Physica C **185−189**, 210 (1991).
[26] D. Shi, H. E. Kourous, M. Xu, and D. H. Kim, Phys. Rev. B **43**, 514 (1991).

[27] Wan-Seon Kim, W. N. Kang, Mun-Seog Kim, and Sung-Ik Lee, Phys. Rev. B **61**, 11 317 (2000).

[28] T. T. M. Palstra, B. Batlogg, R. B. van Dover, L. F. Schneemeyer, and J. V. Waszczak, Phys. Rev. B **41**, 6621 (1990).

[29] C. W. Hagen and R. Griessen, Phys. Rev. Lett. **62**, 2857 (1989).

[30] O. Brunner, M. G. Karkut, L. Antognazza, L. Miéville, P. van der Linden, J. A. A. J. Perenboom, J.-M. Triscone, and Ø. Fischer, Physica C **185−189**, 2079 (1991).

[31] M. Reedyk, C. V. Stager, T. Timusk, J. S. Xue, and J. E. Greedan, Phys. Rev. B **45**, 10 057 (1992).

[32] O. Brunner, L. Antognazza, J.-M. Triscone, L. Miéville, and Ø. Fischer, Phys. Rev. Lett. **67**, 1354 (1991).

[33] J. W. Ekin and J. R. Clem, Phys. Rev. B **12**, 1753 (1975).

[34] Y. Oreg, P. W. Brouwer, B. D. Simons, and A. Altland, Phys. Rev. Lett. **82**, 1269 (1999).

[35] E. Delmer, A. J. Berlinsky, C. Kallin, G. B. Arnold, and M. R. Beasley, Phys. Rev. Lett. **80**, 2917 (1998).

[36] H.-C. Ri, R. Gross, F. Gollnik, A. Beck, R. P. Huebener, P. Wagner, and H. Adrian, Phys. Rev. B **50**, 3312 (1994).